Microsc. Microanal. 15, 197–203, 2009
doi:10.1017/S1431927609090370

Microscopy AND Microanalysis

Optimizing Electron Backscatter Diffraction of Carbonate Biominerals—Resin Type and Carbon Coating

Alberto Pérez-Huerta* and Maggie Cusack

Department of Geographical and Earth Sciences, University of Glasgow, G12 8QQ Glasgow, UK

Abstract: Electron backscatter diffraction (EBSD) is becoming a widely used technique to determine crystallographic orientation in biogenic carbonates. Despite this use, there is little information available on preparation for the analysis of biogenic carbonates. EBSD data are compared for biogenic aragonite and calcite in the common blue mussel, *Mytilus edulis*, using different types of resin and thicknesses of carbon coating. Results indicate that carbonate biomineral samples provide better EBSD results if they are embedded in resin, particularly epoxy resin. A uniform layer of carbon of 2.5 nm thickness provides sufficient conductivity for EBSD analyses of such insulators to avoid charging without masking the diffracted signal. Diffraction intensity decreases with carbon coating thickness of 5 nm or more. This study demonstrates the importance of optimizing sample preparation for EBSD analyses of insulators such as carbonate biominerals.

Key words: aragonite, calcite, mussel, epoxy, diffraction intensity, nanometer

Introduction

Electron backscatter diffraction (EBSD) is a technique that can determine crystallographic orientation of crystalline and polycrystalline material at high spatial resolution. The advantage of EBSD over transmission electron microcopy or X-ray diffraction is that EBSD analyses are rapid, and it is straightforward to associate microstructural features and crystallographic orientation. EBSD has mainly been applied to conductive materials in the fields of materials science and engineering because the crystallographic texture can strongly influence material properties (Field, 1997; Schwartz et al., 2000). Sample preparation and analysis conditions, including polishing and coating, for EBSD of metals and ceramics are well established (Katrakova & Mücklich, 2001, 2002; Nowell et al., 2005). Materials that are natural insulators (e.g., carbonate biominerals), in principle, are not suitable for the application of EBSD. However, the expedience of EBSD has already been shown for biogenic calcite and aragonite in many groups of organisms including mollusks (e.g., Checa et al., 2006; Dalbeck et al., 2006; Cartwright & Checa, 2007), brachiopods (e.g., Schmahl et al., 2004; Cusack et al., 2008*a*, 2008*b*; Pérez-Huerta & Cusack, 2008), and avian eggshells (Dalbeck & Cusack, 2006). Despite these studies, there is little detailed assessment of sample preparation that is crucial for EBSD analyses of biogenic carbonates, beyond that of grinding and polishing procedures (Cusack et al., 2008*b*). The influence of the choice of resin and the thickness of the carbon coating have not been assessed. Here, we analyze EBSD data from biogenic aragonite and calcite in the common blue mussel, *Mytilus edulis*, using different types of resin. EBSD results are also presented for different thicknesses of carbon coating used for conductivity in carbonate samples.

Received December 5, 2008; accepted March 12, 2009
**Corresponding author*. E-mail: Alberto.PerezHuerta@ges.gla.ac.uk

Materials and Methods

Materials

Specimens of the common blue mussel, *M. edulis*, obtained commercially from the west coast of Scotland, were used in this study. Left valves were cut along the length from posterior to umbo regions exposing the outer calcite layer and the innermost aragonite layer. Three blocks (A, B, C), containing both calcium carbonate polymorphs, with approximate dimensions of 3 × 1 cm, were then obtained for analysis (Fig. 1).

Resin Types

Three samples were not embedded in resin (NR) and 12 blocks were embedded in different types of resin for analysis. Araldite epoxy resin was used in our experiments using two combinations: araldite epoxy resin (ER) (Buehler epoxy resin/hardener with a mix of 50 g of resin and 1 g of hardener) and araldite epoxy resin and gold coating (ERgc). Samples were gold coated after embedding in epoxy resin, and subsequently the gold coating was removed prior to

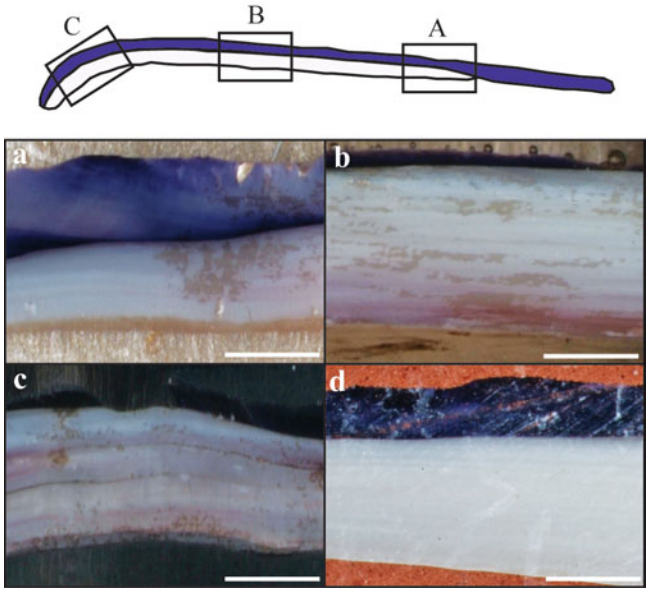

Figure 1. Top: Schematic diagram showing a cut along the length from posterior to umbo regions in *M. edulis*, exposing the outer calcite layer (blue) and the innermost aragonite layer (white), with the position of the sample blocks (A, B, and C). Bottom: Example of shell samples (**a**) without resin and (**b**) embedded in epoxy resin, (**c**) carbon conductive resin, and (**d**) Technovit conductive resin (all scale bars = 1 mm).

Table 1. Assessment of EBSD Results for Aragonite (ar) and Calcite (ca) in Samples A, B, B* (uncoated) and C Embedded in ER, PdR, ERgc, and CB.*

	ER	PdR	ERgc	CB	NR
A (ar)	+	−	+	+	−
A (ca)	+	−	+	+	−
B* (ar)	+	−	−	+	−
B* (ca)	+	−	−	+	−
B (ar)	+	−	+	+	−
B (ca)	+	−	+	+	−
C (ar)	+	−	+	+	+
C (ca)	+	−	+	−	−

*NR blocks were not embedded in resin [presence of diffraction (+) and no diffraction (−)].

carbon coating and analysis. Two conductive resins were also used including a carbon conductive resin (CB) (Buehler epoxyde resin/hardener with a mix of 50 g of resin, 1 g of hardener, and 1 g of potassium carbonate), and a Technovit conductive resin (PdR) (methylmethacrylate-based conductive resin with a mix of 20 g and 13 mL of liquid) (Fig. 1; Table 1).

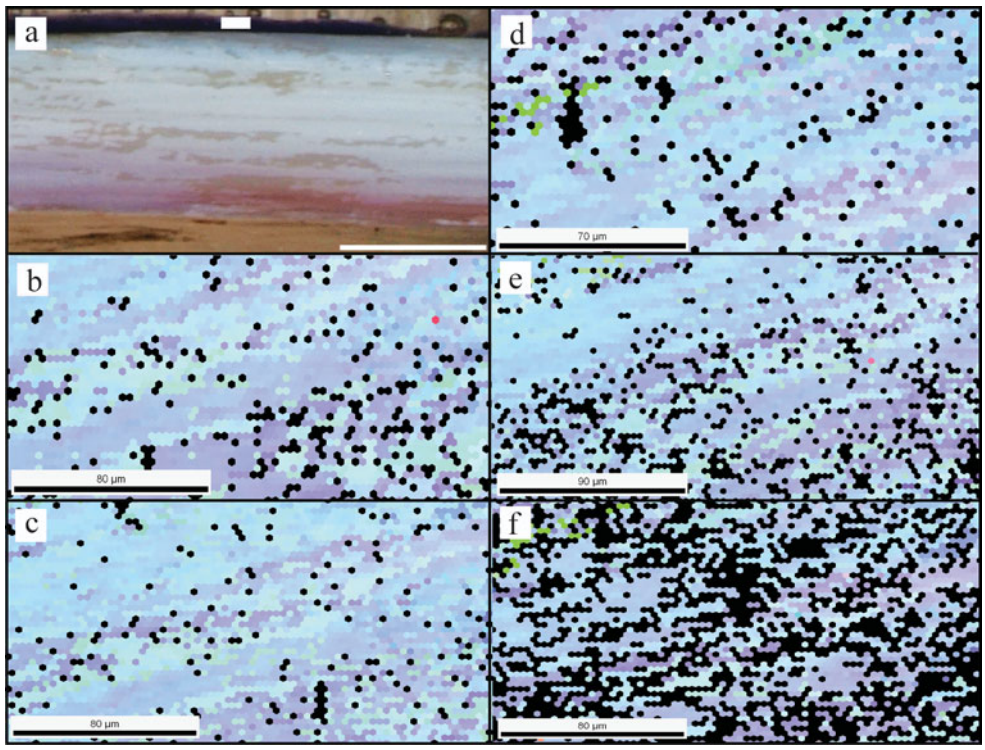

Figure 2. (**a**) EBSD crystallographic orientation maps of a calcite region (white box) in a shell section embedded in epoxy resin. Black dots represent areas of no diffraction. Carbon coat thickness was (**b**) 1.5 nm, (**c**) 2.5 nm, (**d**) 5 nm, (**e**) 10 nm, and (**f**) 15 nm.

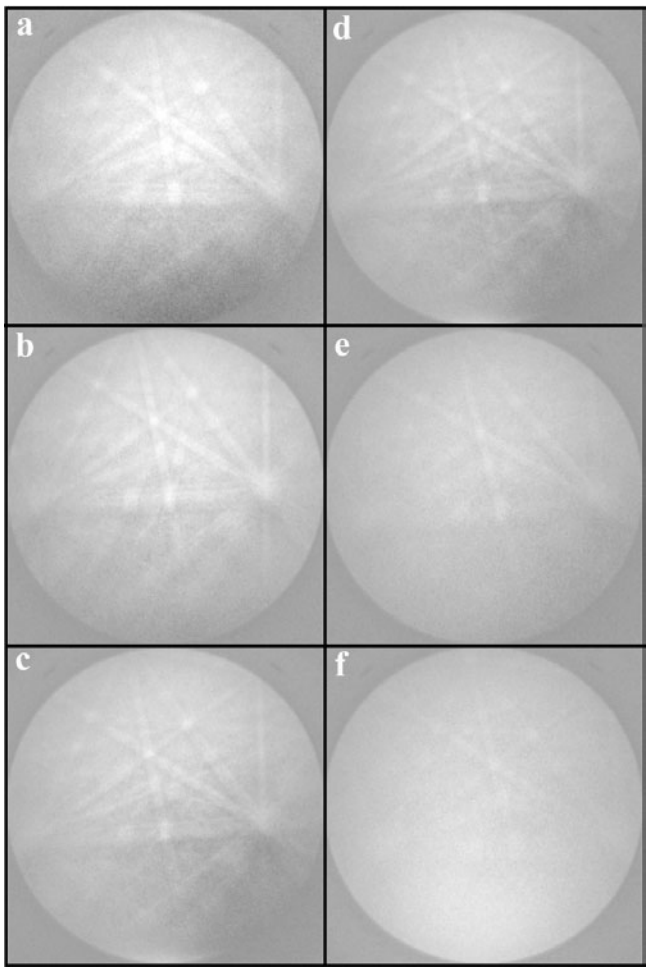

Figure 3. Example of Kikuchi diffraction patterns in calcite for different carbon coating thicknesses: (**a**) 1.5 nm, (**b**) 2.5 nm, (**c,d**) 5 nm, (**e**) 10 nm, and (**f**) 15 nm.

Polishing

Samples were polished prior to analysis through a series of grinding and polishing steps similar to the protocol described in Cusack et al. (2008*b*). Initially, samples were ground using grit papers: P180/220 (82/68 μm; 3 min), P320 (46 μm; 3 min), P800/1000 (21/18 μm; 3 min), P1200 (15 μm; 3 min), P2500 (8 μm; 3 min), and P4000 ($<$5 μm; 5 min). The polishing stages were performed with alpha aluminum oxide at 1 μm and 0.3 μm with final 5 min treatment of 0.06 μm colloidal silica. Finally, samples were cleaned in an ultrasonic bath and dried at room temperature.

Carbon Coating

The thickness of carbon coating was controlled using a Precision Etching-Coating System (Model 682) by Gatan Inc. Two ion guns sputter an ultrathin layer of amorphous carbon on the sample, and an electronic monitor measures the precise thickness of the even carbon layer. Thus a thin and uniform carbon layer was applied to sample surfaces using the following thicknesses: 1.5, 2.5, 5, 7.5, 10, and 15 nm.

Electron Backscatter Diffraction (EBSD)

EBSD was carried out in the Department of Geographical and Earth Sciences at Glasgow University using an FEI Quanta 200F field-emission environmental scanning electron microscope in high (5.5×10^{-6} Torr) and low (5.2×10^{-1} Torr) chamber pressure vacuum modes with an aperture and spot size of 4. The stage was tilted 70°, and the electron beam diffracted by interaction with crystal planes in the shell sample. The diffracted beam interacts with a phosphor screen producing a series of Kikuchi bands that enable crystal identification and orientation to be determined (Dalbeck et al., 2006). Initial analyses to assess different types of resin were carried out using a Digiview camera (EDAX) with 4×4 binning and 500×500 pixel resolution based on an 8-bit grey level data. Subsequent analyses to assess the influence of carbon coating thickness were performed using a Hikari camera (EDAX) with 2×2 binning and 240×240 pixel resolution based on a 12-bit grey level data. Finally, data were analyzed using OIM 5.2 from EDAX-TSL. Maps of crystallographic orientation (Fig. 2) are represented as well as Kikuchi patterns (Fig. 3). Numerical data are also presented for average confidence index (CI) and diffraction intensity (DI).

Results

Resin Types

Three samples were not embedded in resin to compare results from those embedded in resin. There was an absence of diffraction in aragonite and calcite for all blocks with the exception of aragonite in block "C" (Table 1). Although samples were highly polished, the absence of resin generated electron charging that distorted diffraction patterns. In addition, grinding and polishing of samples took longer than for those embedded in resin.

For all resin samples, two sets (six blocks) were embedded in conductive resin. CB resin offered positive results for all samples while the PdR resin, commonly used in metallographic analysis, failed to provide any diffraction data for calcium carbonate shell samples (Table 1). All other samples embedded in ER provided positive results except for those samples uncoated for carbon (B*) and previously coated with gold (see the Materials and Methods section) (Table 1).

After the survey of EBSD for each type of resin, numerical diffraction data were acquired for samples embedded in epoxy resin. Areas of 400×300 μm in aragonite ($\sim$18,500 data points) and 400×250 μm ($\sim$15,400 data points) in calcite were analyzed in each block (A, B, C) to obtain

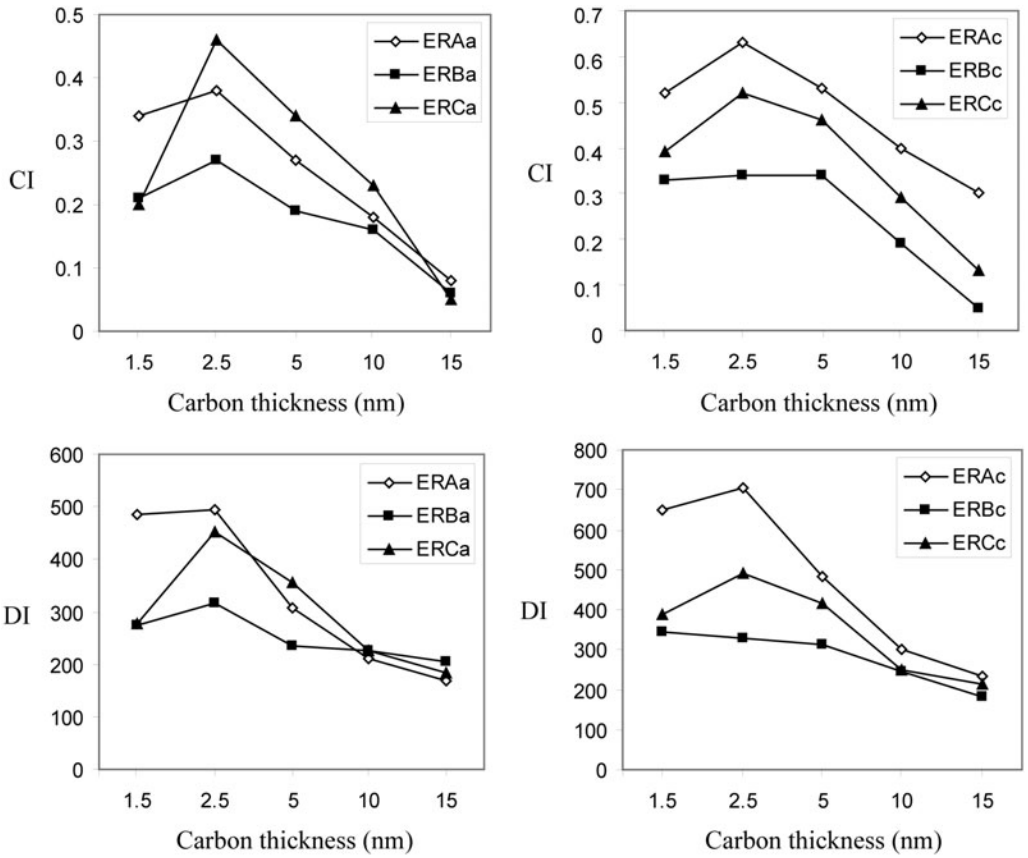

Figure 4. Comparison of average CI and DI values (ar: 45,000 data points) and calcite (ca: 37,500 data points) from carbon coated sample blocks A, B, and C embedded in ER. CI (0-1) and DI (0-1000) are arbitrary units.

Table 2. Average CI and DI Values for Aragonite (ar: 18,500 data points) and Calcite (ca: 15,400 data points).*

	CI (ar)	DI (ar)	CI (ca)	DI (ca)
ER				
A	0.04	18.50	0.07	29.15
B*	0.06	29.42	0.02	38.58
B	0.03	14.36	0.05	17.67
C	0.09	21.65	0.13	33.50
CB				
A	0.07	24.47	0.15	37.35
B*	0.01	21.71	0.03	31.51
B	0.03	16.60	0.07	20.80
C	0.03	14.23	—	—
Ergc				
A	0.07	15.75	0.07	18.75
B*	—	—	—	—
B	0.07	17.82	0.05	20.10
C	0.04	15.58	0.08	23.83

Sample blocks A, B, B (uncoated) and C were embedded in ER, ERgc, and CB and analyzed at a constant carbon thickness value (>10 nm).

average values CI and DI values (Table 2). All analyses yielded positive values of diffraction except for aragonite and calcite in block "C" embedded in CB resin and the carbon uncoated (block "B*") for ERgc resin sample. Average CI and DI values were similar for block samples with different resin types but slightly higher for samples with CB and ER resins (Table 2).

Carbon Coating Thickness

CB and ER resins offered the best results for EBSD. Initially, three sample blocks for each type of resin were coated with a thin layer of carbon between 15–20 nm thick using a vacuum carbon coater. Average CI and DI values were similar in all cases (Table 2). To assess the influence of the thickness of the carbon coat, a high precision carbon coater (Gatan PECS 682), in which a coat of uniform thickness can be controlled at sub-nanometer resolution, was used in subsequent analyses. Aragonite and calcite in each sample block were initially coated with carbon at 1.5 nm thickness, and subsequently this thickness was progressively incremented to perform analysis in the same area at 2.5, 5, 10,

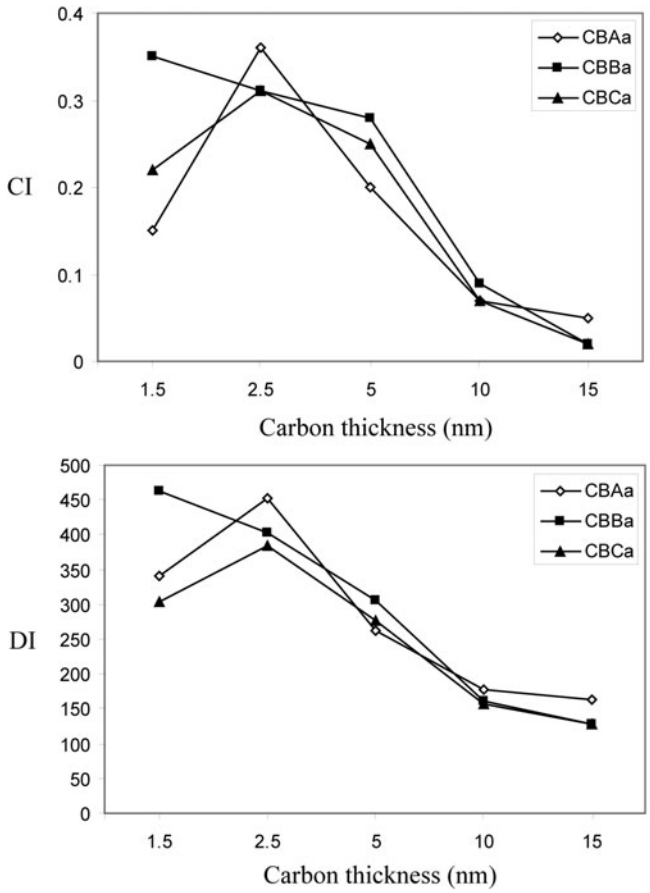

Figure 5. Average CI (0-1) and DI (0-1000) values of carbon coated sample blocks A, B, and C embedded in CB.

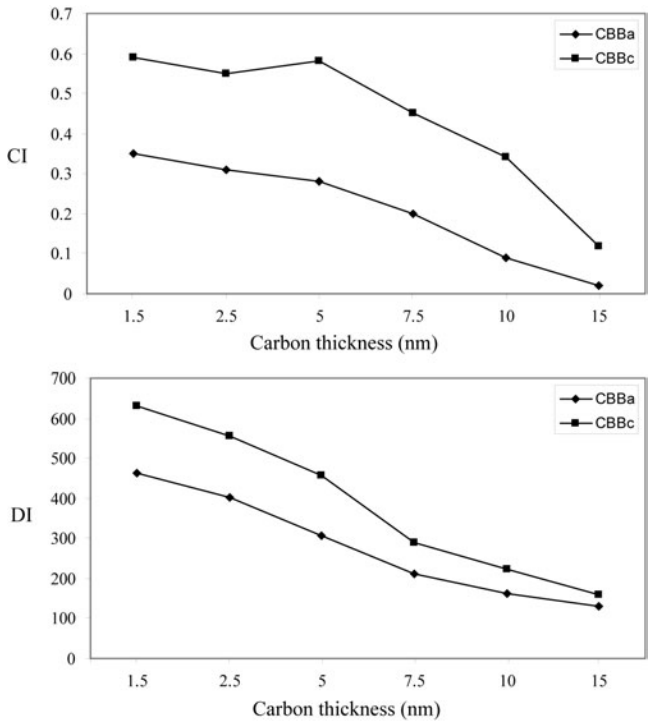

Figure 6. Average CI (0-1) and DI (0-1000) values for aragonite (a) and calcite (c) from block B embedded in CB and coated with carbon.

and 15 nm. Visual data were obtained via crystallographic maps (Fig. 2) and Kikuchi diffraction patterns (Fig. 3). Results show almost no differences when using 1.5, 2.5, and 5 nm in thickness in both cases. In contrast, DI values decrease considerably with 10 and 15 nm carbon thickness (Figs. 2, 3).

Areas of 300 $\times$ 300 μm in aragonite (45,000 data points with measurements every 2 μm) and 400 $\times$ 250 μm (37,500 data points with measurements every 3 μm) in calcite were analyzed in each block (A, B, C) to compare average CI and DI values at different carbon coating thicknesses. For both types of resin (ER and CB), the highest CI and DI values are obtained at 2.5 nm thickness, and there is decline with an increase in carbon thickness reaching almost a value of zero for CI at 15 nm (Figs. 4–6). At 1.5 nm thickness, values are consistently lower than at 2.5 nm because the layer of carbon is very thin resulting in electron charging across the sample surface. Additional measurements at 7.5 nm thickness were conducted in aragonite and calcite of block "B" for CB resin to assess whether the decrease in DI was progressive after 5 nm thickness or more abrupt as suggested with visual data (Figs. 2, 3). Results show that there is a progressive decline in average CI and DI values beyond 5 nm of carbon thickness (Fig. 6).

EBSD analyses were also conducted in the scanning electron microscope (SEM) operating in low vacuum mode to assess the influence of carbon coating thickness with different pressure conditions. Results show good data are obtained for CI and DI with 1.5 and 2.5 nm of carbon thicknesses. However, the quality of diffraction data decreases after 5 nm carbon thickness reaching almost a value of 0 for CI (Fig. 7). A comparison with data obtained in high vacuum mode for aragonite, with the same results for calcite, shows that lower CI and DI values were obtained in low vacuum mode for all carbon thicknesses (Fig. 7).

Discussion

Overall results show that carbonate biomineral samples provide better EBSD results if they are embedded in resin because it facilitates grinding and polishing. The best results were obtained with ER, and the presence of a conductive component in the resin provided no advantage. The most crucial aspect for optimizing EBSD analysis was the thick-

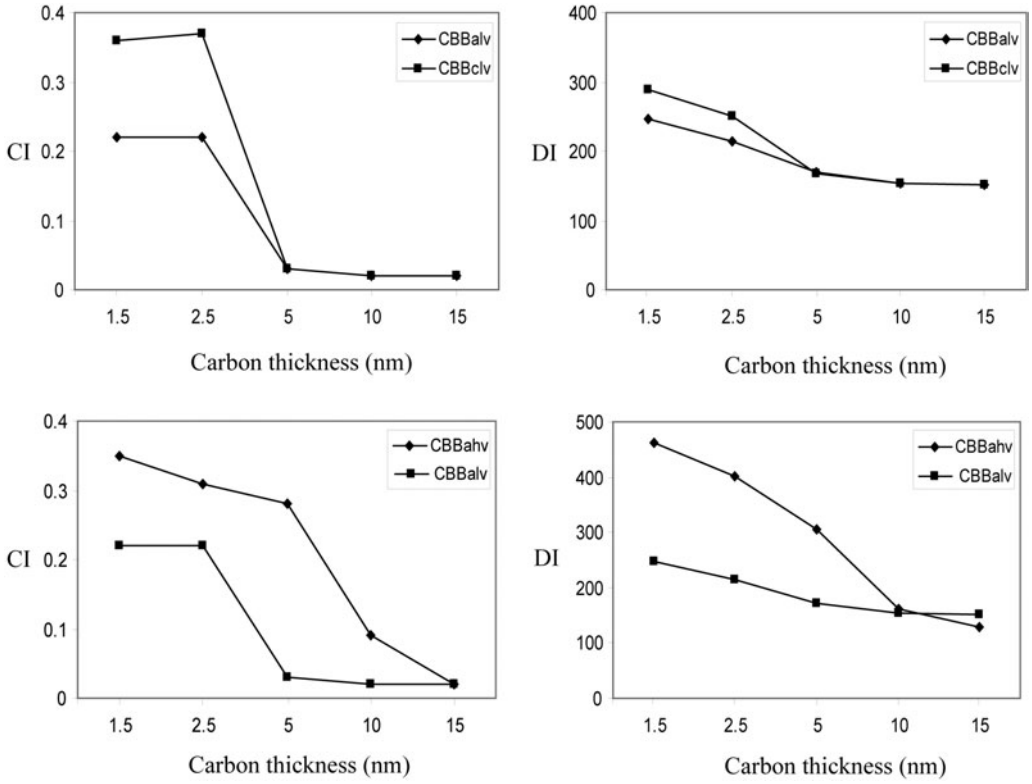

Figure 7. Average CI (0-1) and DI (0-1000) values for aragonite (a) and calcite (c) from block B embedded in CB, coated with carbon and analyzed in low (lv) and high (hv) vacuum modes.

ness of carbon coating used for sample conductivity. Traditional vacuum and sputter carbon coaters tend to lay down an irregular layer of nonuniform thickness. Our results show that a uniform layer of 2.5 nm thickness of carbon gives optimal results and that the intensity of diffraction begins to decrease with more than 5 nm in carbon thickness. Also, our analyses highlight the fact that DI increases in high vacuum mode in contrast to low vacuum mode for all carbon thicknesses. This study demonstrates the importance of technical aspects, such as a resin type and carbon thickness, in the use of EBSD in insulating materials such as biominerals. Further research is needed to understand differences in EBSD results in biominerals for different calcium carbonate polymorphs (aragonite and calcite) and with respect to the influence of organic matter.

Acknowledgments

The authors acknowledge financial support from the Biotechnology and Biological Sciences Research Council (BBSRC) (BB/E003265/1) for this study under the Technology Development Research Initiative. We would like to acknowledge helpful reviews by two anonymous referees and editors, Dr. John Mansfield and Dr. Robert Price, which have improved considerably the quality of this article. We also thank J. Gilleece (sample preparation), Les Hill (photography), and P. Chung (SEM/EBSD).

References

Cartwright, J.H.E. & Checa, A.G. (2007). The dynamics of nacre self-assembly. *J R Soc Interface* **4**, 491–504.

Checa, A.G., Okamoto, T. & Ramírez, J. (2006). Organization pattern of nacre in Pteriidae (Bivalvia: Mollusca) explained by crystal competition. *Proc R Soc B* **273**, 1329–1337.

Cusack, M., Dauphin, Y., Chung, P., Pérez-Huerta, A. & Cuif, J-P. (2008*a*). Multiscale structure of calcite fibres of the shell of the brachiopod *Terebratulina retusa*. *J Struct Biol* **164**, 94–100.

Cusack, M., England, J., Parkinson, D., Dalbeck, P., Lee, M., Curry, G.B. & Fallick, A.E. (2008*b*). Oxygen isotope composition, magnesium, distribution and crystallography of *Terebratulina retusa*. *Fossils & Strata* **54**, 259–267.

Dalbeck, P. & Cusack, M. (2006). Crystallography (electron backscatter diffraction) and chemistry (electron probe microanalysis) of the avian eggshell. *Crys Growth Des* **6**, 2558–2562.

Dalbeck, P., England, J., Cusack, M., Lee, M.R. & Fallick, A.E. (2006). Crystallography and chemistry of the calcium carbonate polymorph switch in *M. edulis* shells. *Eur J Min* **18**, 601–609.

Field, D.P. (1997). Recent advances in the application of orientation imaging. *Ultramicroscopy* **67**, 1–9.

Katrakova, D. & Mücklich, F. (2001). Specimen preparation for electron backscatter diffraction—Part I: Metals. *Practical Metallography* **38**, 547–565.

Katrakova, D. & Mücklich, F. (2002). Specimen preparation for electron backscatter diffraction—Part II: Ceramics. *Practical Metallography* **39**, 644–662.

Nowell, M.M., Witt, R.A. & True, B.W. (2005). EBSD sample preparation: Techniques, tips, and tricks. *Microsc Today* **13**, 44–48.

Pérez-Huerta, A. & Cusack, M. (2008). Common crystal nucleation mechanism in shell formation of two morphologically distinct calcite brachiopods. *Zoology* **111**, 9–15.

Schmahl, W.W., Griesshaber, E., Neuser, R., Lenze, A., Job, R. & Brand, U. (2004). The microstructure of the fibrous layer of terebratulide brachiopod shell calcite. *Eur J Min* **16**, 693–697.

Schwartz, A.J., Kumar, M. & Adams, B.L. (2000). *Electron Backscatter Diffraction in Materials Science*. New York: Kluwer Academic/Plenum Publishers.